The Sorbinil Trap: A Predicted Dead-End Complex Confirms the Mechanism of Aldose Reductase Inhibition†

Kurt M. Bohren* and Charles E. Grimshaw‡

The Harry B. and Aileen Gordon Diabetes Research Laboratory, Molecular Diabetes and Metabolism Section, Department of Pediatrics, Baylor College of Medicine, Houston, Texas 77030 and Signal Pharmaceuticals, San Diego, California 92121

Received April 7, 2000; Revised Manuscript Received June 1, 2000

ABSTRACT: Kinetic and crystallographic studies have demonstrated that negatively charged aldose reductase inhibitors act primarily by binding to the enzyme complexed with oxidized nicotinamide dinucleotide phosphate (E·NADP$^+$) to form a ternary dead-end complex that prevents turnover in the steady state. A recent fluorescence study [Nakano and Petrash (1996) *Biochemistry 35*, 11196−11202], however, has concluded that inhibition by sorbinil, a classic negatively charged aldose reductase inhibitor, results from binding to the enzyme complexed with reduced cofactor (E·NADPH) and not binding to E·NADP$^+$. To resolve this controversy, we present transient kinetic data which show unequivocally that sorbinil binds to E·NADP$^+$ to produce a dead-end complex, the so-called sorbinil trap, which prevents steady-state turnover in the presence of a saturating concentration of aldehyde substrate. The reported fluorescence binding results, which we have confirmed independently, are further shown to be fully consistent with the proposed sorbinil trap mechanism. Our conclusions are supported by KINSIM simulations of both pre-steady-state and steady-state reaction time courses in the presence and absence of sorbinil. Thus, while sorbinil binding indeed occurs to both E·NADPH and E·NADP$^+$, only the latter dead-end complex shows significant inhibition of the steady-state turnover rate. The effect of tight-binding kinetics on the inhibition patterns observed for zopolrestat, another negatively charged inhibitor, is further examined both experimentally and with KINSIM, with the conclusion that all reported aldose reductase inhibition can be rationalized in terms of binding of an alrestatin-like inhibitor at the active site, with no need to postulate a second inhibitor binding site.

Aldose reductase is a monomeric enzyme that catalyzes the NADPH[1]-dependent reduction of a wide variety of carbonyl-containing compounds to their corresponding alcohols. The enzyme follows a classic ordered kinetic mechanism with the coenzyme binding to the enzyme first and leaving last. Recent studies suggest a possible role in osmotic homeostasis (*2*), steroid interconversion (*3*), and detoxification of reactive aldehydes (*4*). The ability of the enzyme to reduce the excess glucose resultant from the hyperglycemia of diabetes mellitus has been linked to diabetic complications affecting the lens, retina, peripheral nerves, and kidney (*5*).

A variety of aldose reductase (*6*) inhibitors (ARIs) developed intensively by the pharmaceutical industry over the last 25 years have been shown to be effective in preventing some of the complications in animal models but were found to be either ineffective or toxic in clinical studies (*7*−*9*). The mechanism of inhibition by these compounds has been the subject of a great deal of confusion in the past. Thus, the uncompetitive or noncompetitive patterns observed for inhibition of the aldehyde reduction reaction by various ARIs has generally led to the conclusion that these compounds do not bind at the active site (*6*, *10*). Those conclusions disregard the possibility that an ARI competing with the alcohol product for binding to the E·NADP$^+$ complex could still bind at the active site and produce the observed inhibition patterns. In fact, the classic tenets of enzyme inhibition pattern prediction outlined in the early 1960s by Cleland (*11*) have been generally ignored by the aldose reductase research community until 1986, when it was noted by Griffin and McNatt that indeed competitive inhibition may be observed with some ARIs if studied in the direction of alcohol oxidation (*12*). Later it was suggested that the patterns observed for inhibition of the closely related aldehyde reductase could be explained if the inhibitor (e.g., sorbinil, alrestatin) were to bind preferentially to the E·NADP$^+$ complex (*13*). This was then confirmed for aldose reductase by Liu et al. (*14*), who also stressed the importance of the prevalent enzyme form in steady state. Subsequently, several atomic structures (*15*−*17*) have clearly shown that ARIs bind to the active site of aldose reductase. Additional studies (*16*, *18*) have confirmed that the coenzyme in these structures is in fact NADP$^+$ and not NADPH. Combining the unique fluorescence properties of alrestatin with site-directed mutagenesis, ultrafiltration (*18*) methods, and an

† This work was supported by the Harry B. and Aileen B. Gordon Foundation; and by NIH GRANT EY11018.

* Corresponding author: Molecular Diabetes and Metabolism Section, Department of Pediatrics, Baylor College of Medicine, 6621 Fannin, Feigin Center MC3-2353, Houston, TX 77030. Phone (713) 770-3759; fax (713) 770-3766; e-mail kbohren@bcm.tmc.edu.

‡ Signal Pharmaceuticals.

[1] Abbreviations: NADPH and NADP$^+$, reduced and oxidized forms of nicotinamide adenine dinucleotide phosphate; ARI, aldose reductase inhibitor.

10.1021/bi000789q CCC: $19.00
Published on Web 07/18/2000

understanding of the key features of the atomic structure, we were able to define the minimum requirements for potent interaction of ARIs with the active site of aldose reductase. Thus, it was clearly established that both alrestatin (*18*) and sorbinil (*19*) bind predominantly to the E·NADP$^+$ complex and cause inhibition by competing with the alcohol substrate. A recent fluorescence study (*20*), however, has arrived at the opposite conclusion, namely, that sorbinil inhibition results from binding to the E·NADPH complex.

In this paper we present stopped-flow kinetic data that show unequivocally that sorbinil exerts its inhibitory effect by binding to E·NADP$^+$ and forming a dead-end complex, the so-called "sorbinil trap". In addition, we have confirmed the results from the fluorescence study in question and shown them to be fully consistent with the proposed inhibition mechanism. Simulations conducted with KINSIM (*21*) support our conclusions and further reinforce the fact that caution must be exercised when classic steady-state inhibition rules are applied to enzymes such as aldose reductase when operating under tight-binding inhibition conditions.

MATERIALS AND METHODS

Materials. Recombinant human aldose reductase was prepared and purified as previously described (*22*). Enzyme was stripped of all nucleotide by the method of Ehrig et al. (*18*) and the protein concentration was estimated from $\epsilon^{280nm} = 48.2$ mM^{-1} cm^{-1} based on the known amino acid composition and published extinction coefficients for Trp (5.69 mM^{-1} cm^{-1}) and Tyr (1.28 mM^{-1} cm^{-1}) residues (*23*). The accuracy of this method has been confirmed by active-site titration with NADPH. D-Xylose, xylitol, NADPH, and NADP$^+$ were purchased from Sigma, and the best available grades of other chemicals and biochemicals were used without further purification. Solutions were prepared from Milli-Q deionized water, and pH was measured with a Radiometer PHM 84 pH meter with a GK 2321C combined electrode.

Stopped-Flow Kinetic Experiments. A Bio-Logic MPS-51 stopped-flow instrument equipped with MOS-1000 modular optical system including a 150 W Hg−Xe lamp (absorbance and fluorescence detection), three syringes, a path length of 1 cm, and a dead time of 2 ms, along with Bio-Kine rapid kinetics data acquisition and analysis software, were used to obtain transient data. Reactions were conducted at 25 °C in 33 mM sodium phosphate buffer (pH 8) containing 0.5 mM sodium ethylenediaminetetraacetate (Na_2EDTA) and 0.1 mM dithiothreitol (DTT). For measurement of multiple-turnover transients, the three syringes contained (1) 150 mM D-xylose and 200 μM sorbinil in standard phosphate buffer, (2) 150 mM D-xylose in standard phosphate buffer, and (3) 20 μM enzyme and 200 μM NADPH in standard phosphate buffer. Use of D-xylose in both syringes 1 and 2 allowed for convenient variation of the final sorbinil concentration, while a constant final D-xylose concentration was maintained. Concentrations given in figures represent the final concentrations in the reaction mixtures. Reduction of xylose was monitored as the change in absorbance at 340 nm assuming identical extinction coefficients for free and enzyme-bound NADPH ($\epsilon = 6.22$ mM^{-1} cm^{-1}).

Initial Velocity Studies. Conventional steady-state initial velocities for hAR-mediated D-xylose reduction or xylitol oxidation were monitored as the rate of enzyme-dependent decrease or increase, respectively, in NADPH absorbance at 340 nm ($\epsilon = 6.22$ mM^{-1} cm^{-1}) on a Gilford Response spectrophotometer at 25 °C. Assays were routinely conducted in duplicate in 1 mL of 0.1 M phosphate buffer, pH 7.0, and monitored for 1 min. All rates were corrected for any background rate (≤5%) detected in the absence of enzyme or substrate. Kinetic constants were calculated by fitting the initial velocities to the appropriate equation in hyperbolic form by unweighted least-squares analysis in SigmaPlot for Windows, version 2.0. Apparent inhibition constants K_{is} and K_{ii} were obtained by using the following general initial velocity equation for noncompetitive inhibition:

$$v_i = VA/[K_a(1 + I/K_{is}) + A(1 + I/K_{ii})] \qquad (1)$$

where K_{is} is the slope inhibition constant, K_{ii} is the intercept inhibition constant, V is the maximal velocity, A is the substrate concentration, I is the inhibitor concentration, and K_a is the Michaelis−Menten constant. The nomenclature used is that of Cleland (*11*). The equations for linear competitive and linear uncompetitive inhibition can be obtained from this general equation by setting $K_{ii} = \infty$ or $K_{is} = \infty$, respectively.

Kinetic Simulations. Reaction progress curves were calculated via the kinetic simulation program KINSIM[2] (*21*) as modified for use under Windows 3.1 by Drs. Bryce V. Plapp and Gary X. Hua using the previously determined microscopic rate constants (*24*) and actual starting concentrations of enzyme, coenzyme, substrate and inhibitor, as indicated. Steady-state initial velocities were obtained from the linear part (30−60 s) of the reaction progress curves, and the data were analyzed as described above. The Δ time was set to 0.03 s, flux and integral tolerance were kept at 0.1 and 0.0001, respectively.

Fluorescence Titrations. To evaluate the findings of Nakano and Petrash (*20*), fluorescence titrations were carried out at 25 °C on an Aminco Bowman series II luminescence spectrophotometer equipped with a thermostated cuvette turret with 1 cm quartz cuvettes. The same triple buffer system was used at pH 7.0 consisting of 25 mM 2-(*N*-morpholino)ethanesulfonic acid, 25 mM potassium phosphate, and 90 mM Tris. Since it was not possible to measure sorbinil fluorescence at 310 nm upon excitation at 285 nm in the presence of 300 μM NADPH, the concentration of NADPH was lowered to 30 μM, which is still saturating. The collected scans (emission 300−345 nm, excitation 285 nm) were analyzed as described previously (*20*).

RESULTS

Stopped-Flow Inhibition Kinetics. The complete reaction mechanism of human aldose reductase is outlined in Scheme 1 as determined previously by steady-state and stopped-flow kinetic experiments, where E is hAR (human aldose reductase), RCHO is D-xylose, RCH_2OH is xylitol, and *E is the isomerized form of the enzyme (*24*). Two additional steps

[2] The KINSIM program for DOS and Windows is freely downloadable from the following web site: http://www.biochem.wustl.edu/cflab/message.html.

Scheme 1

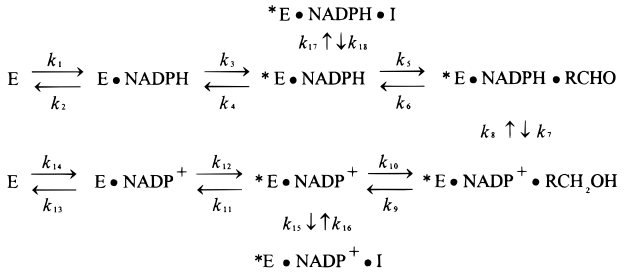

Table 1. Rate Constants for the Reduction of D-Xylose (Forward) and Oxidation of Xylitol (Reverse) by hAR[a]

	forward		reverse
k_1	1.2×10^8 M^{-1} s^{-1}	k_2	174 s^{-1}
k_3	89 s^{-1}	k_4	0.83 s^{-1} (8.3 s^{-1})
k_5	220 M^{-1} s^{-1} (2.2×10^6 M^{-1} s^{-1})	k_6	25 s^{-1} (2500 s^{-1})
k_7	130 s^{-1}	k_8	0.60 s^{-1} (60 s^{-1})
k_9	1.0×10^6 s^{-1} (1.0×10^5 s^{-1})	k_{10}	5×10^6 M^{-1} s^{-1}
k_{11}	0.23 s^{-1} (230 s^{-1})	k_{12}	150 s^{-1}
k_{13}	623 s^{-1}	k_{14}	2.0×10^8 M^{-1} s^{-1}
$K_{d1} = k_{16}/k_{15}$	(for values see text)		
$K_{d2} = k_{18}/k_{17}$	(for values see text)		

[a] In 33 mM sodium phosphate buffer, pH 8.0 (*24*). Values in parentheses were used for the simulation of initial velocities for a model enzyme with modified kinetic properties.

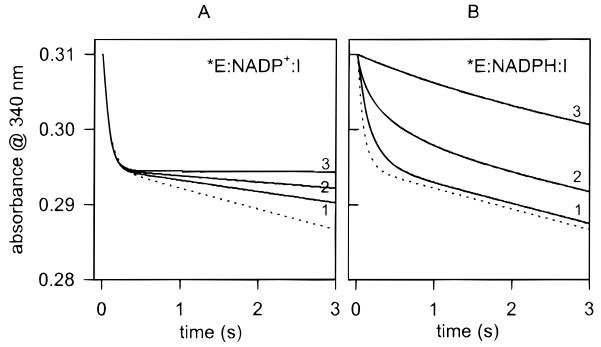

FIGURE 1: Simulated stopped-flow progress curves for hAR-catalyzed D-xylose-dependent NADPH oxidation in the absence (dotted line) and presence (solid lines) of an inhibitor that can bind to either the *E·NADP$^+$ complex (panel A) or the *E·NADPH complex (panel B) with $K_d = 1$ μM (curves 1 and 3) or $K_d = 0.1$ μM (curve 2). The reactions were simulated with the rate constants from Table 1 with 5 μM enzyme, 75 mM aldehyde substrate, and 50 μM NADPH. The concentration of inhibitor is 5 μM (curves 1 and 2) or 50 μM (curve 3).

have been included to allow for inhibitor binding to *E·NADP$^+$ and *E·NADPH, respectively, where I is a classical negatively charged alrestatin-like aldose reductase inhibitor (*18*). The most remarkable feature of this mechanism in the direction of aldehyde reduction is the isomerization step (k_{11}) that precedes nucleotide exchange. This isomerization step is more than 500-fold slower (Table 1) than the chemical step (k_7) that includes hydride and proton transfer, and thus it is the slowest step in the forward direction. As a result, a pre-steady-state burst of enzyme-bound NADP$^+$ formation is readily observed in single- and multiple-turnover experiments (*24*). Figure 1 (dotted lines) shows the simulation by KINSIM using the rate constants in Table 1 of the progress curve for D-xylose reduction by aldose reductase. The simulation displays "burst kinetics" with an initial rapid decline in NADPH absorbance reflecting the fast chemical step (k_7), followed by a much slower steady-state rate corresponding to the isomerization step that precedes exchange of NADP$^+$ with NADPH to complete the turnover cycle. Calculations show that during steady-state turnover with saturating aldehyde substrate more than 99% of the total enzyme is present in the *E·NADP$^+$ form.

On the basis of this mechanism, we can predict that the effect on the pre-steady-state burst phase and on the steady-state phase of the reaction will be quite different depending on whether an inhibitor binds predominantly to *E·NADP$^+$ or to *E·NADPH. Thus, an inhibitor that exerts its effect exclusively by binding to the *E·NADP$^+$ form of the enzyme will have no effect on the pre-steady-state burst but will inhibit the steady-state phase of the reaction by preventing the release of NADP$^+$. On the other hand, an inhibitor that binds only to *E·NADPH will affect both the initial burst and the steady-state phases of the reaction. The effect of increasing aldehyde substrate concentration will also be different in the two cases. Increasing aldehyde concentration will enhance inhibition of the steady-state rate by increasing the fraction of total enzyme present as the *E·NADP$^+$ complex during turnover, if this is the complex that binds inhibitor. By contrast, because aldehyde substrate and inhibitor compete for binding to the same complex, increasing aldehyde concentration will alleviate inhibition of both the burst phase and the steady-state reaction rate if inhibition results from binding to *E·NADPH.

These predictions were confirmed by simulation with KINSIM. The two scenarios where inhibitor binds exclusively to either *E·NADP$^+$ or *E·NADPH were simulated by use of the kinetic mechanism shown as Scheme 1. The rate constant values chosen for the on rate ($k_{15} = k_{17} = 10^8$ M^{-1} s^{-1}) and off rate ($k_{16} = k_{18} = 100$ s^{-1}) for inhibitor binding to either *E·NADP$^+$ (k_{15} and k_{16}) or *E·NADPH (k_{17} and k_{18}) are fast compared to the slowest rates in the overall mechanism to avoid complexities that arise from slow-binding inhibitors (*25*, *26*). The dissociation constant ($K_d = k_{16}/k_{15} = k_{18}/k_{17} = 1$ μM) is based on experimental results.[3] For simulations involving inhibitor binding to one of the binary enzyme nucleotide complexes, the rate constant values for binding to the other complex were set equal to zero.

The results of the simulations for binding to *E·NADP$^+$ and *E·NADPH are shown in Figure 1 panels A and B, respectively. As expected, the progress curves in the absence of inhibitor are identical, showing an initial burst of NADPH oxidation, followed by a much slower steady-state rate (dotted lines). However, in the presence of inhibitor the two modes of inhibition behave quite differently. In the case where the inhibitor binds to *E·NADP$^+$, the rate of the initial burst phase is unchanged, but the steady-state rate is decreased in a dose-dependent manner [solid lines 1 (5 μM inhibitor) and 3 (50 μM inhibitor) in Figure 1A]. In sharp contrast, simulation of the reaction with inhibitor binding to *E·NADPH shows that the initial burst rate is diminished or completely eliminated, with a much smaller effect on the steady-state reaction rate [solid lines 1 (5 μM inhibitor) and 3 (50 μM inhibitor) in Figure 1B]. As expected, decreasing

[3] An apparent K_{ii} of 1.4 ± 0.06 μM was determined experimentally for the inhibitor sorbinil with DL-glyceraldehyde as substrate in 0.1 M phosphate buffer at pH 7.0.

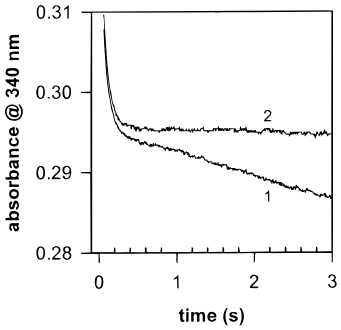

FIGURE 2: Traces of actual stopped-flow experiments with 5 μM hAR (apoenzyme), 75 mM D-xylose, and 50 μM NADPH in the absence (trace 1) or presence (trace 2) of 50 μM sorbinil.

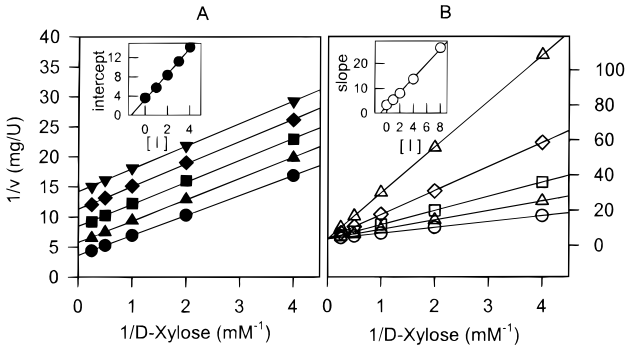

FIGURE 3: Simulated classical steady state: Double-reciprocal representation of simulated steady-state inhibition patterns for the reduction reaction catalyzed by hAR based on rate constants in Table 1. The inhibitor binds to either the *E·NADP$^+$ complex (panel A) or the *E·NADPH complex (panel B) with a K_d of 1 μM. The enzyme concentration is 1 μM and the inhibitor concentration is 0 (●), 1 (▲), 2 (■), 3 (◆), or 4 (▼) μM, respectively (panel A), and 0 (○), 1 (Δ), 2(□), 4 (◇), or 8 (▽) μM, respectively (panel B). Insets show secondary plots of intercept (panel A) or slope (panel B) vs inhibitor concentration, respectively.

K_d further to 0.1 μM by setting $k_{16} = k_{18} = 10$ s^{-1} while keeping the inhibitor concentration at 5 μM leads to a similar effect as simply increasing the concentration of inhibitor at a given K_d (line 2 in Figure 1 panels A and B).

The actual experimental results are shown in Figure 2, where we used recombinant human aldose reductase that had been stripped of any tightly bound nucleotide (*18*) prior to the stopped-flow experiments. High concentrations of enzyme (5 μM), substrates (50 μM NADPH, 75 mM D-xylose), and inhibitor (50 μM sorbinil) were chosen to observe the most dramatic effect. The two stopped-flow progress curves obtained in the presence and absence of inhibitor are identical to the simulations shown in Figure 1A. Specifically, the initial burst of NADPH oxidation is unaffected, while the steady-state rate is almost totally inhibited in the presence of 50 μM sorbinil. Thus, sorbinil effectively traps the enzyme in a dead-end *E·NADP$^+$·ARI complex from which NADP$^+$ release is completely prevented. Calculations show that the roughly 2% remaining steady-state activity observed at this concentration of sorbinil corresponds precisely to the amount of enzyme not trapped in the dead-end complex.

Steady-State Inhibition Kinetics. If negatively charged aldose reductase inhibitors such as sorbinil, tolrestat, alrestatin, zopolrestat, and citrate exert their inhibitory effect by binding to the *E·NADP$^+$ complex, the rules of classical steady-state inhibition theory (*11*) predict uncompetitive inhibition versus aldehyde substrate in the forward reaction and competitive inhibition versus the alcohol substrate in the reverse reaction. Conversely, if the ARI inhibits by binding to *E·NADPH the predictions are reversed: competitive inhibition versus aldehyde in the forward reaction and uncompetitive inhibition versus alcohol in the reverse reaction. If ARI binding can occur to both E·nucleotide complexes, the result will be noncompetitive inhibition versus either aldehyde or alcohol substrate. The relative contribution of the slope (K_{is}, competitive) and intercept (K_{ii}, uncompetitive) inhibition components in each case will be determined primarily by two factors: (1) the dissociation constant for the *E·nucleotide·ARI complex (e.g., $K_d = k_{16}/k_{15}$ for *E·NADP$^+$·ARI complex in Scheme 1) responsible for the inhibition and (2) the fraction of total enzyme present in the proper form (e.g., *E·NADP$^+$) during steady-state turnover. K_d is a direct measure of binding affinity and reflects the chemistry of the active-site interaction between, for example, *E·NADP$^+$ and sorbinil. The fraction of enzyme present in a particular form (e.g., *E·NADP$^+$) during steady-state turnover will be a function of the substrate concentrations and the relative rates of various steps in the enzyme kinetic mechanism.

Inhibition patterns versus aldehyde substrate reported in the literature for inhibition of aldose reductase include uncompetitive and noncompetitive patterns, depending on the inhibitor used. These patterns have been interpreted to mean either that ARIs do not bind at the enzyme active site (*6*, *10*), that the conformational change associated with nucleotide exchange is responsible (*15*), that ARIs bind to both *E·NADP$^+$ and *E·NADPH (*19*), that competition between substrate and inhibitor is masked in the overall rate of the reaction (*27*), or that tight binding causes noncompetitive inhibition patterns (*20*). The validity of some of these interpretations is questionable in the light of structural and direct binding data, which clearly demonstrate that ARIs bind at the active site, predominantly when NADP$^+$ is present. To determine the basis for noncompetitive inhibition patterns observed with human aldose reductase, we have used KINSIM to simulate the steady-state inhibition of aldose reductase by sorbinil and zopolrestat, two well-characterized aldose reductase inhibitors. Since KINSIM does not invoke any steady-state assumptions, the validity of a steady-state treatment can be evaluated.

Initial simulations were conducted with the microscopic rate constants determined previously for human aldose reductase and assuming a K_d value of 1 μM for sorbinil binding to either *E·NADP$^+$ or *E·NADPH. This value is based on the K_d of 0.3 μM for alrestatin binding to *E·NADP$^+$ determined by fluorescence titration and the K_{ii} of 1.4 ± 0.06 μM for sorbinil inhibition versus aldehyde substrate.[3] Simulated initial velocities obtained with KINSIM for the case where ARI binds exclusively to *E·NADP$^+$ are shown plotted in double-reciprocal form in Figure 3A. The figure, with discrete points indicating concentrations for which simulations were run and which might practically be used for in vitro experiments, shows a typical uncompetitive inhibition pattern as predicted by classical steady-state inhibition rules. Fitting eq 1 to the data with $K_{is} = \infty$ gave a K_{ii} of 1.36 ± 0.04 μM. Simulation of the reverse alcohol oxidation reaction using the same model gave the predicted competitive inhibition pattern with K_{is} of 1.34 ± 0.06 μM

(data not shown). The K_{ii} versus aldehyde and K_{is} versus alcohol values are equal because (1) both inhibition constants represent binding to the same *E·NADP$^+$ complex and (2) during steady-state turnover the fraction of total enzyme present as *E·NADP$^+$ is nearly 100% both at saturating aldehyde concentration (conditions where K_{ii} versus aldehyde is determined) and at very low alcohol concentration (conditions where K_{is} versus alcohol is determined).

With the alternative model where ARI binds exclusively to *E·NADPH, the resulting inhibition patterns are again as predicted. Thus, in the aldehyde reduction direction the simulations show competitive inhibition with a K_{is} of 1.34 ± 0.06 μM (Figure 3B), while in the reverse reaction the results display uncompetitive inhibition versus alcohol substrate with a K_{ii} of 9.2 ± 0.2 μM (data not shown). The higher value for K_{ii} versus alcohol as compared to K_{is} versus aldehyde is directly related to the steady-state fraction of enzyme present as the ARI-binding *E·NADPH complex under the reaction conditions where the two inhibition constants are measured. Thus, only 15% of the enzyme is present as *E·NADPH at saturating alcohol concentration (conditions where K_{ii} versus alcohol is determined) (*24*), which is 7-fold lower than the nearly 100% of total enzyme present as *E·NADPH at very low aldehyde concentration (conditions where K_{is} versus aldehyde is determined).

To simulate the model where ARI can bind to both *E·nucleotide complexes, we have set the K_d for sorbinil binding to *E·NADP$^+$ at 1 μM and that for binding to *E·NADPH at 15 μM. Graphical analysis of the sorbinil versus aldehyde inhibition pattern reported by Petrash and Nakano (*20*) gives apparent K_{ii} (0.25 μM) and K_{is} (3.5 μM) values that reflect a 15-fold lower binding affinity for *E·NADPH. Similar relative binding affinities for binding to *E·NADP$^+$ versus *E·NADPH have been reported for other negatively charged ARIs, i.e., alrestatin (*18*) and mandelate (*19*). The simulation results show a noncompetitive inhibition pattern versus D-xylose ($K_{is} = 9.8 \pm 2.8$ μM, $K_{ii} = 1.46 \pm 0.05$ μM) and a nearly competitive inhibition pattern versus xylitol ($K_{is} = 1.6 \pm 0.1$ μM, $K_{ii} = 19.4 \pm 3.3$ μM). The intercept component is practically absent for inhibition versus xylitol because of two factors (1) 15-fold higher K_d for binding to *E·NADPH versus *E·NADP$^+$ and (2) 7-fold lower fraction of total enzyme present as the *E·NADPH complex during steady-state turnover. The net result is that the apparent K_{ii} value is more than an order of magnitude greater than K_{is} and thus kinetically negligible and practically not detectable. Note that the simulated inhibition pattern versus D-xylose exactly mimics the pattern reported previously for sorbinil inhibition versus DL-glyceraldehyde (*20*), confirming that sorbinil inhibition occurs predominantly via binding to *E·NADP$^+$, with a much smaller contribution at low aldehyde concentrations from ARI binding to *E·NADPH.

Tight-Binding Inhibition Kinetics. To simulate the inhibition patterns observed under tight-binding conditions, we decreased K_d for ARI binding 1000-fold, from 1 μM to 1 nM (e.g., $k_{15} = 10^8$ M^{-1} s^{-1} and $k_{16} = 0.1$ s^{-1}), and simulated initial rates as a function of substrate and inhibitor concentration as before. As predicted by tight-binding inhibition theories (*28*, *29*), the resulting inhibition patterns appeared indentical, regardless of which E·nucleotide complex was responsible for ARI binding and which substrate, aldehyde or alcohol, was varied. The simulated inhibition patterns for reaction in the D-xylose reduction and xylitol oxidation direction for both models display noncompetitive patterns in double-reciprocal plot representations (Figure 4). Closer inspection of the slope and intercept replots (insets, Figure 4), however, clearly reveals the nonlinearity that is characteristic of tight-binding inhibition (*28*, *29*). At very high aldehyde substrate concentrations, the simulated inhibition pattern for the model where ARI binds to *E·NADPH displays downward curvature due to the ability of aldehyde to compete with ARI for binding at the enzyme active site (not shown). This type of downward curvature at high substrate concentrations is predicted by the tight-binding inhibition theory (*28*) but is often difficult to confirm experimentally.

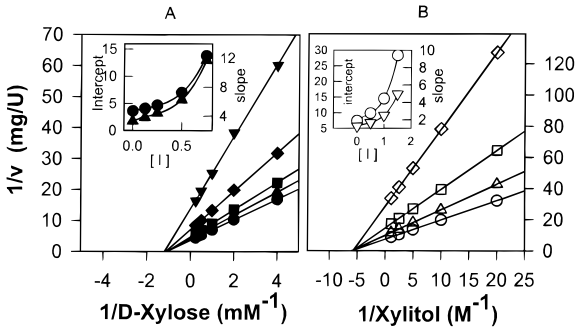

FIGURE 4: Simulated tight binding: Double-reciprocal representation of simulated steady-state inhibition patterns for the reduction (panel A) and oxidation (panel B) reactions, respectively, catalyzed by hAR based on rate constants in Table 1. The patterns shown are the same whether inhibitor binds to the *E·NADP$^+$ complex or to the *E·NADPH complex, with K_d equal to 1 nM. The enzyme concentration is 1 μM (panel A) or 2 μM (panel B) and the inhibitor concentration is 0 (●), 125 (▲), 250 (■), 500 (◆), or 750 (▼) nM, respectively (panel A), and 0 (○), 0.5 (Δ), 1.0 (□), or 1.5 (◇) μM, respectively (panel B). Insets show secondary plots of slopes and intercepts vs inhibitor concentration.

To test this kind of inhibition in vitro we used the negatively charged inhibitor zopolrestat, which binds very tightly to the active site of aldose reductase (*30*, *15*). As predicted for a tight-binding inhibitor, the experimentally observed inhibition pattern for zopolrestat versus D-xylose (Figure 5A) is noncompetitive. The inhibition pattern for zopolrestat versus xylitol in the oxidation reaction direction shows a similar noncompetitive pattern (Figure 5B). The slope and intercept replots are nonlinear, as expected. What is obvious is that the *type* of inhibition pattern observed (e.g., competitive, noncompetitive, uncompetitive) for a tight-binding inhibitor such as zopolrestat is of no help in establishing the *E·nucleotide complex primarily responsible for ARI binding.

General Case. The conclusions reached thus far are based on the rather unusual kinetic properties of human aldose reductase (*24*). To examine the more general case, and the relation of observed kinetic patterns to actual binding events for inhibition where $K_d < E_t$, we modified certain rate constants for the ordered bi-bi mechanism in Scheme 1 to obtain a more "typical" enzyme with kinetic parameters shown in Table 2. The main difference between this model enzyme mechanism and that for human aldose reductase in the forward aldehyde reduction direction is that turnover is much faster (38 s^{-1} versus 0.19 s^{-1}) and the chemical step, not nucleotide exchange, is now largely rate-limiting. In

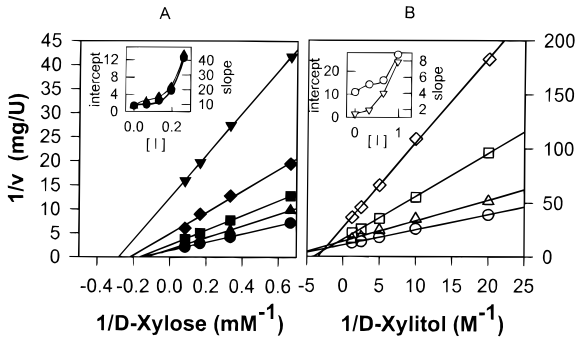

FIGURE 5: Experimental: Double-reciprocal representation of steady-state inhibition patterns determined experimentally for the reduction (panel A) and oxidation (panel B) reaction catalyzed by hAR and inhibited by zopolrestat in 0.1 M sodium phosphate, pH 7.0. The enzyme concentration is 0.33 μM (panel A) or 1.7 μM (panel B) and the inhibitor concentration is 0 (●), 65 (▲), 130 (■), 195 (◆) or 260 (▼) nM, respectively (panel A), and 0 (○), 325 (Δ), 650 (□), or 975 (◇) nM, respectively (panel B). Insets show secondary plots of slopes and intercepts vs inhibitor concentration.

Table 2. Calculated Kinetic Parameters

	hAR	model
V_1/E_t (s^{-1})	0.19	38
K_a (μM)	0.005	1.0
K_b (mM)	1.0	0.35
K_{dNADPH} (μM)	0.013	0.12
V_2/E_t (s^{-1})	0.08	4.7
K_q (μM)	0.003	2.2
K_p (mM)	169	4.4
K_{dNADP+} (μM)	0.005	1.9

addition, binding of the aldehyde substrate (k_5/k_6 ratio) has been increased 100-fold compared to human aldose reductase. In the reverse alcohol oxidation direction, nucleotide exchange has become largely rate limiting for the model enzyme reaction, whereas for aldose reductase the rate-limitation is distributed about equally between the nucleotide exchange and chemical steps. To mimic conditions that would yield reasonable experimental initial velocities in vitro, we chose 5 nM and 50 nM as the enzyme concentration for simulation of the forward and reverse reactions, respectively.

Evaluation of the KINSIM results for the model enzyme shows that the inhibition patterns obtained were precisely those predicted on the basis of classical steady-state inhibition rules (*11*), provided the K_d for inhibitor was ≥10 nM. This was true regardless of which *E·nucleotide complex bound ARI. As soon as the K_d value decreased significantly below 10 nM, however, the inhibition patterns obtained from the simulations shifted back to the noncompetitive pattern with nonlinear slope and intercept replots characteristic of tight-binding inhibition, like that observed for aldose reductase inhibition by zopolrestat. Our KINSIM simulations thus confirm one of the basic tenets of tight-binding inhibition theory, namely, that it is the ratio of K_d/E_t which indicates whether one is operating in the tight-binding inhibition regime. When assay conditions are such that the inhibitor binds very tightly to the enzyme ($K_d \ll E_t$) or the enzyme concentration required to obtain measurable rates in vitro is very high relative to the inhibitor potency ($E_t \gg K_d$), then tight-binding inhibition kinetics may apply and interpretation of experimentally determined inhibition patterns based on the classical steady-state inhibition rules can be misleading.

Sorbinil Fluorescence Binding Study. Recently it was reported that binding of sorbinil to an E·NADPH complex of human aldose reductase results in fluorescence enhancement (excitation 285 nm, emission 310 nm) with an apparent K_d of 1.7 μM (*20*). Because titration of the analogous E·NADP$^+$ complex did not show any fluorescence enhancement, the proposal was made that sorbinil binding, and thus sorbinil inhibition, derives solely from binding to an E·NADPH complex and does not involve any binding to E·NADP$^+$. We have been able to reproduce these fluorescence titration results by using a modified experimental protocol (30 μM instead of 300 μM nucleotide to reduce inner filter effects) and have confirmed that sorbinil binding does indeed result in fluorescence enhancement for E·NADPH but not for E·NADP$^+$ (data not shown).

Our interpretation of these results is quite different from the previous proposal (*20*). Thus, the absence of a fluorescence change does not preclude sorbinil binding to *E·NADP$^+$. Rather, this result simply requires that sorbinil binding to form a ternary *E·NADP$^+$·sorbinil complex must be silent fluorescently. Similarly, sorbinil binding to *E·NADPH with an apparent K_d of 1.7 μM does not prove that this *E·NADPH·sorbinil complex is responsible for the observed inhibition of the enzymatic reaction. On the basis of our stopped-flow and steady-state kinetic data and the results from extensive KINSIM simulations, we would argue that sorbinil binding to *E·NADPH does lead to weak inhibition but that the primary effect comes from the ternary *E·NADP$^+$·sorbinil complex.

DISCUSSION

Although the mechanism of inhibition by classical aldose reductase inhibitors (sorbinil, alrestatin, citrate, tolrestat, zopolrestat) has been described in great detail (*16*, *18*, *19*), there is still confusion regarding why different inhibition patterns are observed, ranging from uncompetitive to noncompetitive in the aldehyde reduction direction and from competitive to noncompetitive in the alcohol oxidation direction. In particular, a recent study (*20*) concluded that sorbinil inhibition results from binding to E·NADPH and not E·NADP$^+$, in direct conflict with previous crystallographic and kinetic studies of human aldose reductase. In the present paper, we use pre-steady-state and steady-state kinetic results, combined with extensive KINSIM simulations, to conclusively demonstrate that the primary mode of inhibition for negatively charged ARIs derives from binding of the ARI at the enzyme active site to the *E·NADP$^+$ complex. Furthermore, this mechanism of inhibition can account for all reported steady-state inhibition by alrestatin-like (*18*) inhibitors and all crystallographic and inhibitor binding results without the need to invoke any additional ARI binding sites.

The sorbinil trap experiment was inspired by extensive stopped-flow experimentation that lead to a detailed kinetic mechanism for human aldose reductase, including all the relevant microscopic rate constants (*24*). The remarkably slow rate of exchange of NADP$^+$ with NADPH compared to the fast chemistry of the reduction reaction for human aldose reductase results in an initial pre-steady-state burst of NADPH oxidation that has been observed and quantified (*24*). The ability to measure the effect of an ARI, such as

sorbinil, on both the pre-steady-state burst and the steady-state turnover of aldehyde reduction reaction provides an ideal opportunity to identify precisely which E·nucleotide complex is primarily responsible for ARI inhibition. Thus, the burst phase of the reaction monitors only those steps from the addition of aldehyde to *E·NADPH (k_5) through the oxidation of NADPH (k_7) and does not involve the *E·$NADP^+$ complex at all. Conversely, because steady-state turnover is limited by the rate of the isomerization step preceding nucleotide exchange (k_{11}), this rate is largely controlled by the fate of the *E·$NADP^+$ complex. Both the experimental data (Figure 2) and the KINSIM simulation (Figure 1A) clearly demonstrate that it is the combination of ARI with *E·$NADP^+$ that leads to inhibition of the steady-state turnover rate for human aldose reductase.

The next point of confusion relates to the inhibition patterns reported for various ARIs in the literature. To address this point, KINSIM simulations were performed with the aldose reductase kinetic mechanism and assuming that the ARI can bind exclusively either to *E·$NADP^+$ or to *E·NADPH. For inhibitors with K_d values 1 μM and above, the resulting inhibition patterns are precisely those predicted on the basis of the classical rules for steady-state inhibition (*11*). Specifically, an ARI binding only to *E·$NADP^+$ displays uncompetitive inhibition in the forward direction and competitive inhibition in the reverse direction, with an apparent K_{ii} value for inhibition versus aldehyde equal to the apparent K_{is} value for inhibition versus the alcohol substrate, respectively. Inhibition by citrate shows exactly this pattern for inhibition of human aldose reductase (*16*).

In some cases, the inhibitor may display some affinity for binding to the *E·NADPH complex as well, and this will result in a small but measurable slope effect for inhibition versus the aldehyde substrate in the forward reaction. Graphical analysis of the data reported for sorbinil inhibition of human aldose reductase (*20*) indicates that binding to *E·NADPH under their reaction conditions is roughly 15-fold weaker than binding to *E·$NADP^+$ (compare $K_{is} = 3.5$ μM versus $K_{ii} = 0.25$ μM). A similar 10-fold preference for binding of DL-mandelate to *E·$NADP^+$ relative to *E·NADPH has been reported for the C298A mutant of human aldose reductase (*19*). In fact, KINSIM simulation of such a model where sorbinil binding to *E·$NADP^+$ is 15-fold tighter than binding to *E·NADPH exactly reproduces the published inhibition pattern (*20*). The preferred binding of anionic inhibitors to *E·$NADP^+$ arises from the distinct anion binding site formed by key active-site residues in the vicinity of the nicotinamide C4 position (*16*). This anion binding site and its relation to inhibitor binding and catalysis has been discussed in detail elsewhere (*19*).

The final point of confusion arises when the potency of the ARI increases to the point where the classical rules of steady-state inhibition no longer apply and the rules of tight-binding inhibition take over. As others have discussed (*1*, *28*, *29*) and we have shown directly by KINSIM simulation, the key factor is the K_d/E_t ratio. Typically, the classical steady-state inhibition rules can be used to predict the inhibition patterns as long as $K_d/E_t \geq 10$. Below that value, inhibitor depletion due to binding can no longer be ignored and the steady-state equations break down. Because the turnover number for aldose reductase catalysis is very low, high concentrations ($\sim$1 μM) of enzyme are required to obtain measurable rates from the absorbance change of NADPH oxidation. As a result, inhibition patterns can begin to show the effects of tight binding for ARIs with binding constants in the 1 μM range. If one uses NADPH fluorescence, however, one can decrease the amount of aldose reductase required to obtain measurable rates about 10-fold, with the result that ARIs in the 1 μM potency range no longer display tight-binding inhibition patterns.[4] A similar effect was shown for the model enzyme where, because the amount of enzyme used in the simulations was reduced to only 5 nM, tight-binding kinetic effects were only observed when the K_d for ARI binding was decreased below 10 nM.

Once the K_d/E_t ratio has decreased to the point that tight-binding kinetics apply, identical noncompetitive inhibition are observed regardless of which E·nucleotide complex binds the ARI or which reaction direction is studied. We have confirmed this by both KINSIM simulation (Figure 4) and experimentally with zopolrestat (Figure 5). Intuitively, this makes sense since the net effect of a noncompetitive inhibitor is to make it seem as if less enzyme were present (*31*). Thus, any tight-binding ligand capable of trapping a particular enzyme form in a dead-end complex (e.g., *E·$NADP^+$·ARI) will inhibit the enzymatic reaction by a factor of $1 - [I_t]/[E_t]$, effectively reducing the available enzyme molecules that can participate in the catalytic cycle.[5] In general this statement can be applied to any kinetic mechanism. The actual K_d value below which tight-binding kinetics will apply, however, will depend not only on the total enzyme concentration but also on the relative rates of various steps in the kinetic mechanism involved in substrate binding, inhibitor binding, and catalysis (*26*).

To summarize, pre-steady-state and steady-state kinetic experiments and KINSIM simulations conclusively demonstrate that inhibition by negatively charged ARIs results primarily from binding at the enzyme active site to form an *E·$NADP^+$·ARI dead-end complex. This mechanism of inhibition is consistent with the steady-state inhibition patterns reported for various ARIs, which show limited potency ($K_d \geq 1$ μM), and is also consistent with previous crystallographic, kinetic, and inhibitor binding results. For compounds displaying greater potency, such as zopolrestat, where the K_d values are such that the rules of tight-binding inhibition must be applied in order to correctly analyze the experimental data, the observed inhibition patterns can still be accounted for without invoking the need for any additional ARI binding site.

[4] This effect of lower aldose reductase enzyme concentration has been confirmed experimentally by comparing inhibition patterns determined fluorometrically (classical) with those measured spectrophotometrically (nonclassical tight-binding) with 10-fold more enzyme (Grimshaw and Lai, unpublished results).

[5] Inhibition of this type has been termed stoichiometric (*1*).

ACKNOWLEDGMENT

We thank Dr. Bryce V. Plapp for generously making available his laboratory for the stopped-flow kinetic experiments.

REFERENCES

1. Werkheiser, W. C. (1961) *J. Biol. Chem. 236*, 888−893.
2. Burg, M. B. (1988) *Kidney Int. 33*, 635−641

3. Wermuth, B., and Monder, C. (1983) *Eur. J. Biochem. 131*, 423−426.
4. Vander Jagt, D. L., Robinson, B., Taylor, K. K., and Hunsaker, L. A. (1992) *J. Biol. Chem. 267*, 4364−4369.
5. Gabbay, K. H. (1973) *N. Engl. J. Med. 288*, 831−836.
6. Kador, P. F., Robison, W. G. J., and Kinoshita, J. H. (1985) *Annu. Rev. Pharmacol. Toxicol. 25*, 691−714.
7. Dvornik, D. (1987) *Aldose Reductase Inhibition*, McGraw-Hill, New York.
8. Sarges, R., and Oates, P. J. (1993) *Prog. Drug. Res. 40*, 99−161.
9. Pfeifer, M. A., Schumer, M. P., and Gelber, D. A. (1997) *Diabetes 46*, Suppl-9.
10. Lee, Y. S., Pearlstein, R., and Kador, P. F. (1994) *J. Med. Chem. 37*, 787−792.
11. Cleland, W. W. (1963) *Biochim. Biophys. Acta 67*, 188−196.
12. Griffin, B. W. and McNatt, L. G. (1986) *Arch. Biochem, Biophys, 246*, 75−81.
13. DeJongh, K. S., Schofield, P. J., and Edwards, M. R. (1987) *Biochem. J. 242*, 143−150.
14. Liu, S. Q., Bhatnagar, A., and Srivastava, S. K. (1992) *Biochem. Pharmacol. 44*, 2427−2429.
15. Wilson, D. K., Tarle, I., Petrash, J. M., and Quiocho, F. A. (1993) *Proc. Natl. Acad. Sci. U.S.A. 90*, 9847−9851.
16. Harrison, D. H., Bohren, K. M., Ringe, D., Petsko, G. A., and Gabbay, K. H. (1994) *Biochemistry 33*, 2011−2020.
17. Urzhumtsev, A., Tete-Favier, F., Mitschler, A., Barbanton, J., Barth, P., Urzhumtseva, L., Biellmann, J. F., Podjarny, A., and Moras, D. (1997) *Structure 5*, 601−612.
18. Ehrig, T., Bohren, K. M., Prendergast, F. G., and Gabbay, K. H. (1994) *Biochemistry 33*, 7157−7165.
19. Grimshaw, C. E., Bohren, K. M., Lai, C. J., and Gabbay, K. H. (1995) *Biochemistry 34*, 14374−14384.
20. Nakano, T., and Petrash, J. M. (1996) *Biochemistry 35*, 11196−11202.
21. Barshop, B. A., Wrenn, R. F., and Frieden, C. (1983) *Anal. Biochem. 130*, 134−145.
22. Bohren, K. M., Page, J. L., Shankar, R., Henry, S. P., and Gabbay, K. H. (1991) *J. Biol. Chem. 266*, 24031−24037.
23. Gill, S. C., and von Hippel, P. H. (1989) *Anal. Biochem. 182*, 319−326.
24. Grimshaw, C. E., Bohren, K. M., Lai, C. J., and Gabbay, K. H. (1995) *Biochemistry 34*, 14356−14365.
25. Morrison, J. F., and Walsh, C. T. (1988) *Adv. Enzymol. Relat. Areas Mol. Biol. 61*, 201−301.
26. Sculley, M. J., Morrison, J. F., and Cleland, W. W. (1996) *Biochim. Biophys. Acta 1298*, 78−86.
27. Sugiyama, K., Chen, Z., Lee, Y. S., and Kador, P. F. (2000) *Biochem. Pharmacol. 59*, 329−336.
28. Morrison, J. F. (1969) *Biochim. Biophys. Acta 185*, 269−286.
29. Cha, S. (1975) *Biochem. Pharmacol. 24*, 2177−2185.
30. Mylari, B. L., Beyer, T. A., Scott, P. J., Aldinger, C. E., Dee, M. F., Siegel, T. W., and Zembrowski, W. J. (1992) *J. Med. Chem. 35*, 457−465.
31. Segel, I. H. (1993) *Enzyme Kinetics*, John Wiley & Sons, Inc.

BI000789Q